Source of the Chaoyangzhai Gold Deposit, Southeast Guizhou: Constraints from LA-ICP-MS Zircon U–Pb Dating, Whole-rock Geochemistry and *In Situ* Sulfur Isotopes

Hinyuen Tsang [1,2], Jingya Cao [1,2,]* and Xiaoyong Yang [1,2,]*

[1] CAS Key laboratory of Crust-Mantle Materials and Environments,
University of Science and Technology of China, Hefei 230026, China; geotsang2012@yahoo.com.hk

[2] CAS Center for Excellence in Comparative Planetology, University of Science and Technology of China,
Hefei 230026, China

* Correspondence: jingyacao@126.com (J.C.); xyyang@ustc.edu.cn (X.Y.);
Tel.: +86-0551-360-6871 (J.C.); +86-0551-360-6871 (X.Y.)

Abstract: The Chaoyangzhai gold deposit is one of the newly discovered medium to large scale turbidite-hosted gold deposits in Southeast Guizhou, South China. In this study, laser ablation-inductively coupled plasma-mass spectrometer (LA-ICP-MS) zircon U–Pb dating on the tuffaceous- and sandy-slates of Qingshuijiang Formation, Xiajiang Group, and gold-bearing quartz vein yielded similar age distributions, indicating that zircon grains in gold-bearing quartz vein originated from the surrounding tuffaceous- and sandy-slates. In addition, the youngest weighted mean ages of the zircon grains from the tuffaceous- and sandy-slates were 775 ± 13 Ma and 777 ± 16 Ma, respectively, displaying that the tuffaceous- and sandy-slates of the Qingshuijiang Formation were likely deposited in Neoproterozoic. Based on their major and trace element compositions, the tuffaceous- and sandy-slates were sourced from a felsic igneous provenance. The sandy slates have higher contents of Au (mostly ranging from 0.019 to 0.252 ppm), than those of the tuffaceous slates (mostly lower than 0.005 ppm). The $\delta^{34}S_{V\text{-}CDT}$ values of pyrite and arsenopyrite of the gold-bearing samples range from +8.12‰ to +9.99‰ and from +9.78 to +10.78‰, respectively, indicating that the sulfur source was from the metamorphic rocks. Together with the evidence of similar geochemical patterns between the tuffaceous- and sandy-slates and gold-bearing quartz, it is proposed that the gold might be mainly sourced from sandy slates. The metamorphic devolatilization, which was caused by the Caledonian orogeny (Xuefeng Orogenic Event), resulted in the formation of the ore-forming fluid. Gold was likely deposited in the fractures due to changes of the physico-chemical conditions, leading to the formation of the Chaoyangzhai gold deposit, and the large-scale gold mineralization in Southeast Guizhou.

Keywords: zircon U–Pb age; in situ sulfur isotopes; gold source; ore genesis; Chaoyangzhai gold deposit; Southeast Guizhou

1. Introduction

The turbidite-hosted gold deposit, belonging to the orogenic class of gold deposits, was first explored in Australia and Canada [1–3]. Quartz vein type ore bodies of turbidite-hosted gold deposit commonly occur in the metamorphic rocks and they are related to the faults and/or shear zones [4]. In addition, these gold deposits often appear in groups and/or belts, which are characterized by abundant gold resources and reserves. Examples include Hill End in central New South Wales,

Australia [3], the Bendigo-Ballarat in central Victoria, Australia [5], the Suurikuusikko in Central Lapland Greenstone Belt, Finland [6], and Tianzhu-Jinping in southeast Guizhou, China [7–10]. The source of gold for these turbidite-hosted gold deposits has been debated and two contrasting models exist: (1) the metamorphic rocks that host the gold deposits and (2) the gold-rich fluid from the igneous intrusions [11]. However, the viewpoint that gold of these turbidite-hosted gold deposits is sourced from metamorphic rocks has been widely accepted [11–14].

The western Jiangnan Orogenic Belt, which is situated in the Xuefeng region, is one of the most important turbidite-hosted gold belts in South China, with 319 explored gold deposits/mines and an estimated gold reserve of >200 t [15]. The Southeast Guizhou province, together with the west Hunan province, are significant part of the western Jiangnan Orogenic Belt, where numerous of turbidite-hosted gold deposits were explored, such as Bake, Jinjing, Pingqiu, and Kengtou gold deposits (Figure 1) [8–10]. Although some studies have been carried out on these gold deposits, the source and genesis of these deposits are still poorly constrained [8–10]. As a newly discovered turbidite-hosted gold deposit in southeast Guizhou province, the Chaoyangzhai gold deposit has attracted little attention from the geologists. Furthermore, the source and genesis of this deposit still remain unclear. Therefore, a series of laser ablation-inductively coupled plasma-mass spectrometer (LA-ICP-MS) zircon U–Pb dating, bulk-rock major and trace element compositions, and in situ LA-multi-collector-ICP-MS (LA-MC-ICP-MS) sulfur isotopic analyses were carried out for this deposit, with the aim of providing some new insights regarding the source and genesis of this specific gold deposit and the regional style of gold mineralization.
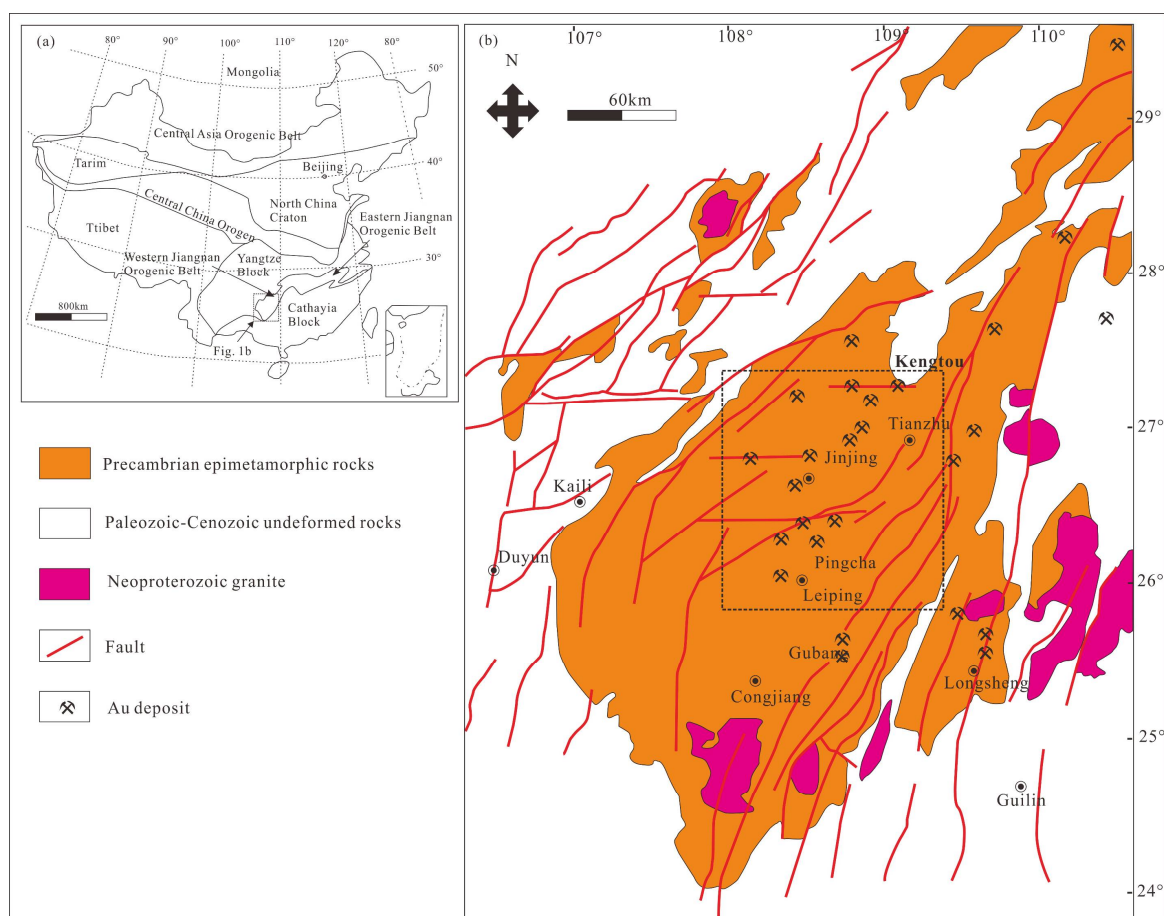

Figure 1. (**a**) Geological sketch map of China (modified from [8,16]); (**b**) Geological map of the western part of Jiangnan Orogenic Belt, showing the location of Precambrian rocks, granitic intrusions and gold deposits (modified from [8,17]).

2. Geological Setting

2.1. Regional Geology

The Jiangnan Orogenic Belt, which extends from northern Guangxi in the southwest to western Zhejiang in the east, 1500 km long, and ca. 500 km wide, was proposed to be the junction zone between the Yangtze and Cathysia Blocks at Neoproterozoic (Figure 1a) [10,18]. This belt can be subdivided into eastern- and western-parts, with distinct types of mineralization. The western part is characterized by gold mineralization that is related to the orogeny, whereas the eastern part is famous for tungsten polymetallic mineralization related to the Yanshanian magmatism [7,10,19–22]. The Southeast Guizhou, which is located at the western part of the Jiangnan Orogenic Belt, is famous for the intense gold mineralization and it is one of the important gold producers in China [7–10,23,24]. The stratigraphic sequences of this area consist of the Neoproterozoic Xiajiang Group (also named Banxi Group in Hunan Province), Sinian, Carboniferous, Permian, Jurassic, Cretaceous, and Quaternary units (Figure 1b). As the basement and the gold-bearing strata, the Xiajiang Group is widespread in this area and it is subdivided into seven formations, of which four are prominent in the Southeast Guizhou Province: the Longli Formation, the Pinglue Formation, the Qingshuijiang Formation and the Fanzhao Formation (Figure 2) [4,25]. The Longli Formation, with a thickness of 1300–1700 m, is mainly composed of blastopsammite, intercalated with blastopsephitic siltstone, blastopsephitic arkose, and silty sericite slate; The Pinglue Formation (1500–2000 m thick) is mainly composed of sericite slate of silty slate, which is intercalated with a few tuffaceous slate and blastopsammite; The Qingshuijiang Formation (2300–3700 m thick) is mainly composed of bluish or gray, thin to medium banded tuffaceous slate, and laminated medium to thick tuff; The Fanzhao Formation (>1000 m thick) can be subdivided into an Upper Formation and a Lower Formation, which comprise tuffaceous slate and blastopsammite, intercalated with banded tuff, and gray slate, intercalated with blastopsammite, respectively.
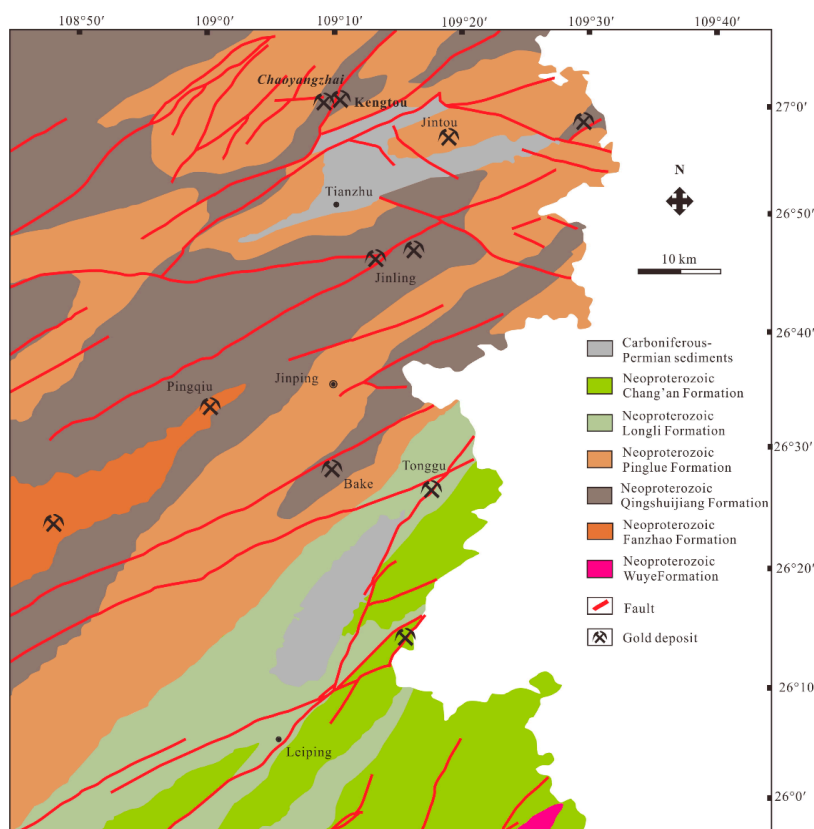

Figure 2. Geological map of the Southeast Guizhou, showing the location of Precambrian rocks, gold deposits (modified from [8,26]).

Multistage tectonic events since the Proterozoic has influenced the Southeast Guizhou [25]. During the Xuefeng movement, a series of NE-trending structures were formed, corresponding to the Jinning Orogeny [27–30]. Subsequently, several EW-trending basement rifts were formed during the Caledonian movement [27–29,31]. Subsequently, a series of NNE-trending faults were formed, which were caused by the subduction of the Pacific plate during the Yanshanian and Himalayan movements [27–29,31]. In addition, these NNE-trending faults overprint the EW- and NE-trending structures, and the current tectonic framework was established in this region [4,25]. The magmatic activity is not intense in this region, and only a few Neoproterozoic granitic plutons were intruded (Figure 1b).

2.2. Ore Deposit Geology

The Chaoyangzhai gold deposit, which was located at Tianzhu County, Southeast Guizhou, is one of the newly found medium to large scale gold deposits in this region, with an estimated gold reserve of 18,442 kg. The ore-bearing strata are the Neoproterozoic epimetamorphic rocks of Qingshuijiang Formation, Xiajiang Group, which are mainly composed of sandy- and tuffaceous-slates (Figures 3 and 4a,b). The sandy slate contains porphyroclastic quartz, plagioclase, and sericite (Figure 4c). The tuffaceous-slate is mainly composed of quartz as the phenocryst and particulate phenocryst as matrix (Figure 4d). The NE-trending faults are widespread in this deposit, and they are mostly trans-tensional normal faults and transpressional reverse thrust faults (Figure 3). These fractures are not only permeable structures but are also the ore-hosting structures.
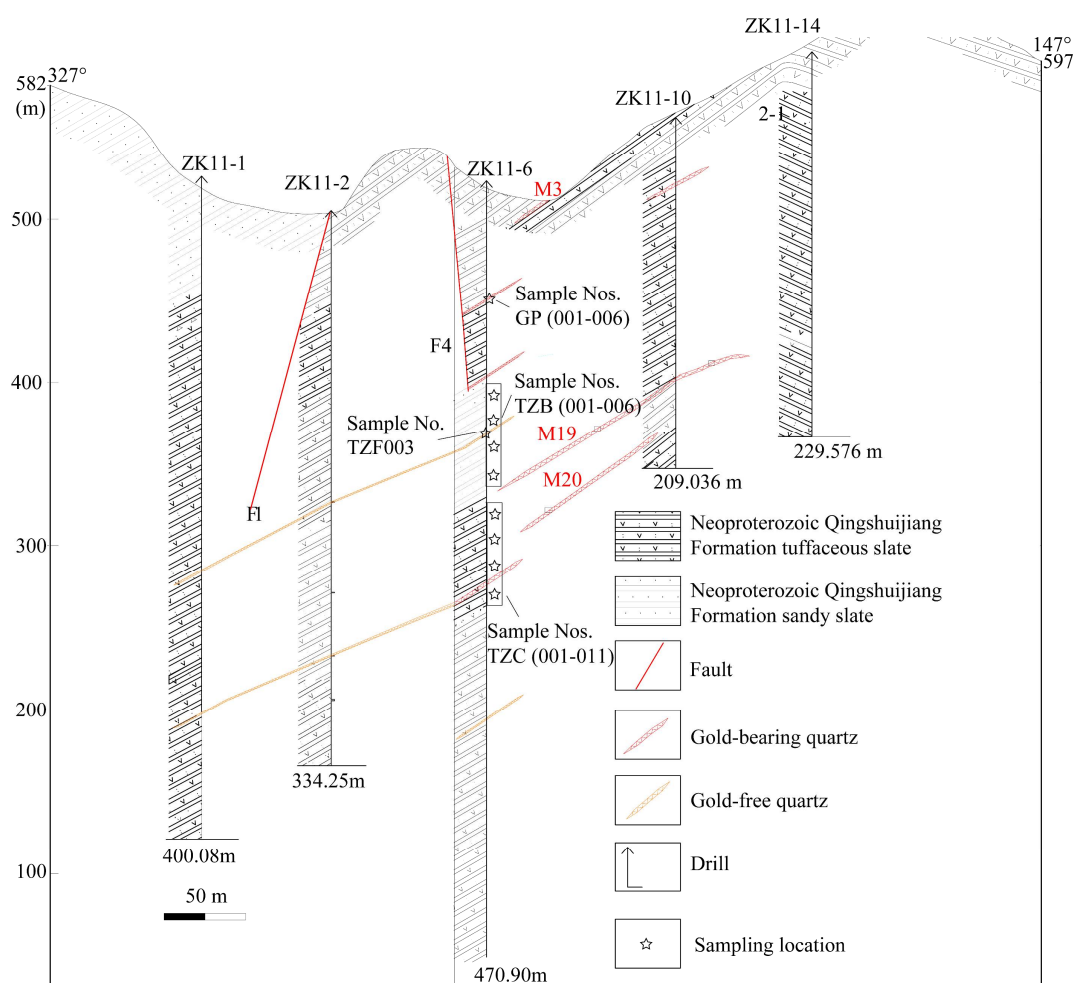

Figure 3. Geological Section of the Chaoyangzhai gold deposit, showing drill-core holes and depths.

A total of over fifty quartz veins are found in this deposit, including eight gold bearing veins. These ore veins are mainly NE-trending, with a length of 200–250 m, a thickness of 0.34–1.40 m (mean = 0.65 m), and an Au grade of 0.58–49.5 g/t (mean = 8.4 g/t). In addition, ore veins can occur in both of the sandy- and tuffaceous-slates (Figure 4a,b). The ore minerals are mainly composed of native gold, arsenopyrite, and pyrite (Figure 4e). Most of the native gold grains are 0.1 mm to 3.0 mm within the quartz veins, in granular and/or irregular form, and they co-exist with the sulfides (Figure 4e). Pyrite commonly occurs in the quartz veins, mostly co-existing with the arsenopyrite, with euhedral or subhedral (Figure 4f). Arsenopyrites are mainly disseminated and occurring in the quartz veins, with euhedral or subhedral, short-columnar and relatively coarse grains (0.5–4 mm) (Figure 4g,h). The gangue minerals include quartz, calcite, mica, and chlorite. In general, similar to those gold deposits in this region, hydrothermal alteration of the Chaoyangzhai gold deposit is subtle, and it mainly consists of silicification and carbonatization [7–9].
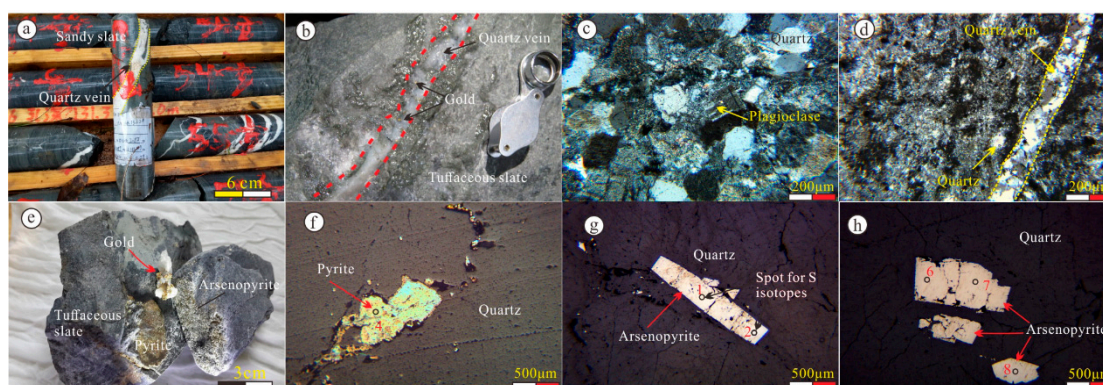

Figure 4. Morphology and mineral assemblages of the surrounding rocks, ore body and gold-bearing ore. (**a**) Quartz vein in the sandy-slate; (**b**) Gold-bearing Quartz vein in the tuffaceous slate; (**c**) Quartz and plagioclase in the sandy-slate; (**d**) Quartz veinlet in the tuffaceous slate; (**e**) Quartz, native gold, pyrite and arsenopyrite in the tuffaceous slate; (**f**) Pyrite in the quartz vein showing the location of the in situ sulfur isotopic analyses; (**g**) Clintheriform arsenopyrite in the quartz vein showing the spots of the in situ sulfur isotopic analyses; and, (**h**) Euhedral arsenopyrite in the quartz vein showing the spots of the in situ sulfur isotopic analyses.

3. Sampling and Analytical Methods

Samples of sandy slate (Sample Nos. TZB001–TZB006 and TZD002), tuffaceous slate (Sample Nos. TZC001–TZC011 and TZD001), gold-free quartz vein (Sample No. TZF003), and gold-bearing quartz veins (Sample Nos. GP1–GP10 and TZD003) were collected from the drill-cores. Figure 3 shows the sampling locations.

3.1. In Situ LA-ICP-MS Zircon U–Pb Dating

Three samples, which were selected for the zircon U–Pb dating, were tuffaceous slate (sample No. TZD001), sandy slate (sample No. TZD002), and gold-bearing quartz vein (sample No. TZD003). Firstly, the zircon grains were separated from these samples and then identified by hand picking under a binocular microscope, mounted in epoxy resin, and polished to expose the interiors. The transmitted and reflected light images of the zircon grains were photographed for documentation (not shown). Cathodoluminescence (CL) images of the zircons were taken while using a scanning micro-probe (JEOL JXA-8100, JEOL, Tokyo, Japan at CAS Key Laboratory of Crust–Mantle Materials and Environments in University of Science and Technology of China, Hefei, China). Zircon U–Pb dating was undertaken with an Agilent 7700 inductively coupled plasma-mass spectrometer (ICP-MS, Agilent, Santa Clara, CA, USA), which was combined with a Coherent 193 laser ablation (LA) system at Sample Solution Analytical Technology Co., Ltd, Wuhan, China. Two zircon standards, 91500 (1062 ± 4 Ma) [32] and GJ-1 (610.0 ± 1.7 Ma) [33], were used as the external standards for dating. Standard silicate glass

(NIST SRM610) was used for external standardization for trace element analysis, and 29Si was used for internal standardization (32.8% SiO$_2$ in zircon). The standard protocol correction method was used in analyzing the 91500 and GJ-1 standard zircons twice and once, respectively, after every five analyses. ICPMSDataCal software was used to process the raw ICP-MS data [34,35], and common Pb was corrected following [36]. Isoplot processed the concordia ages (Version 3.0; [37]).

3.2. Whole Rock Major and Trace Elements Analyses

ALS Geochemistry Laboratory in Guangzhou, China carried out whole rock major and trace elements analyses. Before the analyses, samples were crushed in a steel jaw crusher, and then powdered in an agate mill to grain size of 74 μm. The detailed methodologies for major element compositions are as follows: Loss of ignition (LOI) was determined after igniting sample powders at 1000 °C for 1 h. A calcined or ignited sample (0.9 g) was added to 9.0 g of Lithium Borate Flux (Li$_2$B$_4$O$_7$–LiBO$_2$), mixed well, and then fused in an auto fluxer at 1050 and 1100 °C. A flat molten glass disk was prepared from the resulting melt. A Panalytical Axios Max X-ray fluorescence (XRF, Panalytical, Almelo, The Netherlands) instrument analyzed this disk was then analyzed, with an analytical accuracy of ca. 1–5%. ICP-MS measured the trace element compositions (Perkin Elmer Elan 9000, Perkin, Waltham, MA, USA), with an analytical accuracy better than 5%.

3.3. In Situ LA-MC-ICP-MS Sulfur Isotopic Analyses

In situ sulfur isotopic analyses of pyrite and arsenopyrite were performed using Laser ablation system of a RESOlution M-50 laser ablation system (ASI, Australia), which was equipped with a 193 nm ArF CompexPro102 excimer laser (Coherent, Santa Clara, CA, USA) and Nu Plasma 1700 multi-collector inductively coupled plasma mass spectrometry (MC-ICP-MS, NP-1700, Nu Instruments, Wrexham, UK) in the State Key Laboratory of Continental Dynamics, Northwest University, Xi'an, China. The laser spot sizes of 25–37 μm were used at an energy density of 3.6 J/cm^2 and a repetition rate of 3 Hz. Each analysis included 30 s baseline and 60 s of ablation, with He gas (gas flows = 0.86 L/min) as the carrier gas during the analytical process. Sixteen Faraday cups and three ion counters were used to determine the sulfur isotopic compositions, with a H5 cup for ^{34}S, an Ax cup for ^{33}S, and a L4 cup for ^{32}S. The in-house sulfur reference material (PY-4, δ^{34}S$_{V-CDT}$ = 1.7 ± 0.3‰, [38]) was used for external standard bracketing. The detailed procedures for sulfide in-situ sulfur isotopic analyses were reported in [39,40].

4. Results

4.1. LA-ICP-MS Zircon U–Pb Ages

Table S1 presents the results of LA-ICP-MS zircon U–Pb ages.

Twenty-nine zircon grains from the tuffaceous slate were selected for the LA-ICP-MS U–Pb dating, and most of these selected zircon grains have internal oscillatory zoning, indicating a magmatic origin (Figure 5a,b, [41]). In addition, these zircon grains have Th and U contents of 160–3728 ppm and 126–3754 ppm, respectively, with Th/U ratios of 0.43–1.77. Most of the analyses are concordant, yielding the zircon U–Pb ages of 2731–246 Ma, with a major peak of 795 Ma (Figure 6a). Ten spots of zircon grains have youngest ages of 751–806 Ma, yielding a weighted mean age of 775 ± 13 Ma (MSWD = 0.64, Figure 6b).

Twenty-six zircon grains from the sandy slate sample, with internal oscillatory zoning, were selected for the zircon U–Pb dating (Figure 5c,d). These zircon grains have variable Th and U contents of 47.8–1219 ppm and 126–1176 ppm, respectively, with Th/U ratios of 0.43–3.12. Most of the analyses are concordant, yielding the zircon U–Pb ages of 2604–755 Ma, with a major peak of 815 Ma (Figure 6c). Six spots of zircon grains have the youngest ages of 796–756 Ma, yielding a weighted mean age of 777 ± 16 Ma (MSWD = 0.57, Figure 6d).
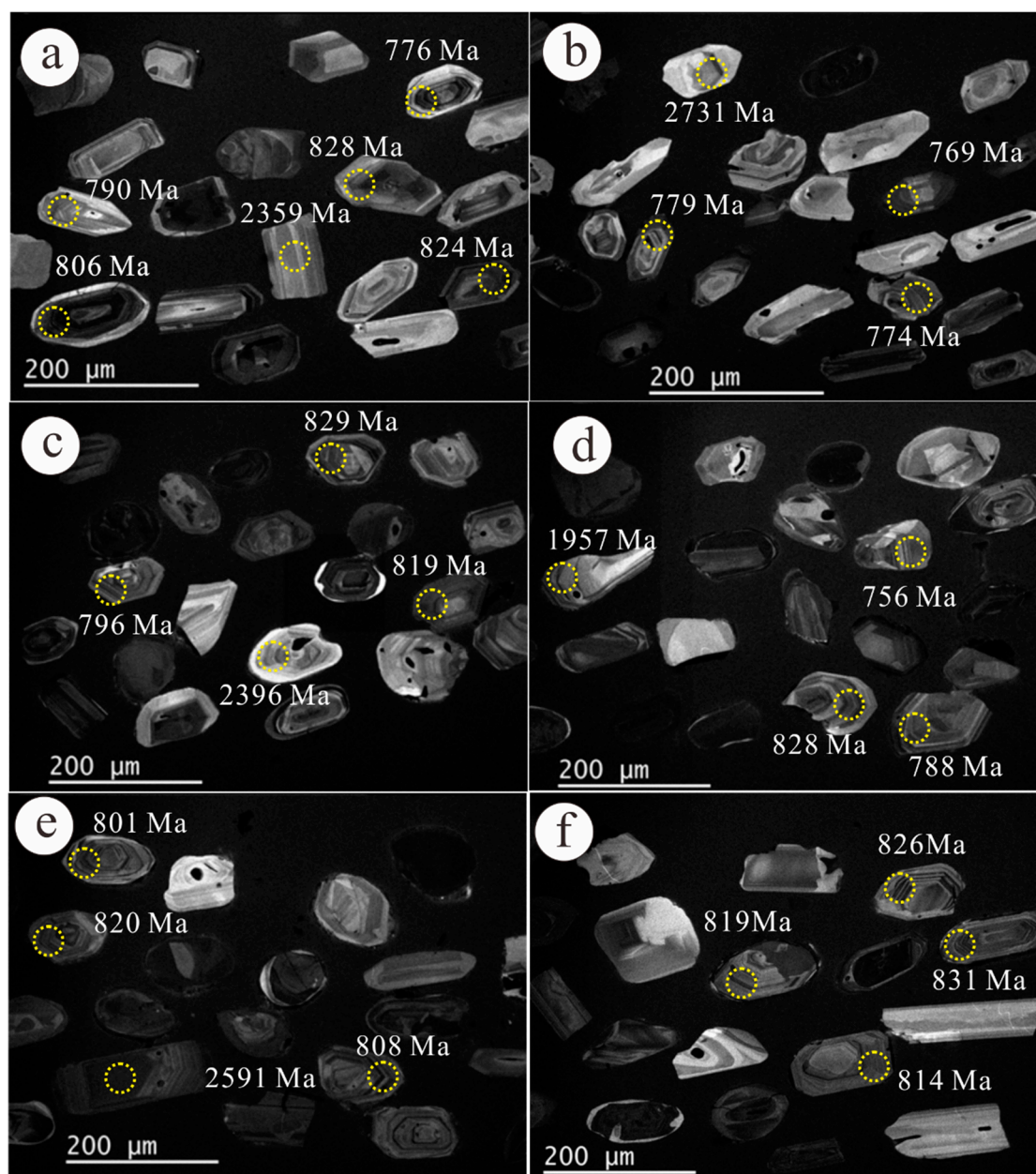
Figure 5. Cathodoluminescence (CL) images of zircon grains from the represented samples, showing the location of the spots for laser ablation-inductively coupled plasma-mass spectrometer (LA-ICP-MS) U–Pb dating. (**a**) and (**b**) are of tuffaceous slate; (**c**); and, (**d**) are of sandy slate; (**e**) and (**f**) are of gold-bearing quartz vein.

Twenty-nine zircon grains from the quartz sample, with internal oscillatory zoning, were selected for the zircon U–Pb dating (Figure 5e,f). These zircon grains have variable Th and U contents of 113–1722 ppm and 168–1442 ppm, respectively, with Th/U ratios of 0.51–2.35. Most of the analyses are concordant, yielding the zircon U–Pb ages of 2683–743 Ma, with a major peak of 810 Ma (Figure 6e). Five spots of zircon grains have youngest ages of 743–814 Ma, yielding a weighted mean age of 773 ± 18 Ma (MSWD = 0.97, Figure 6f).
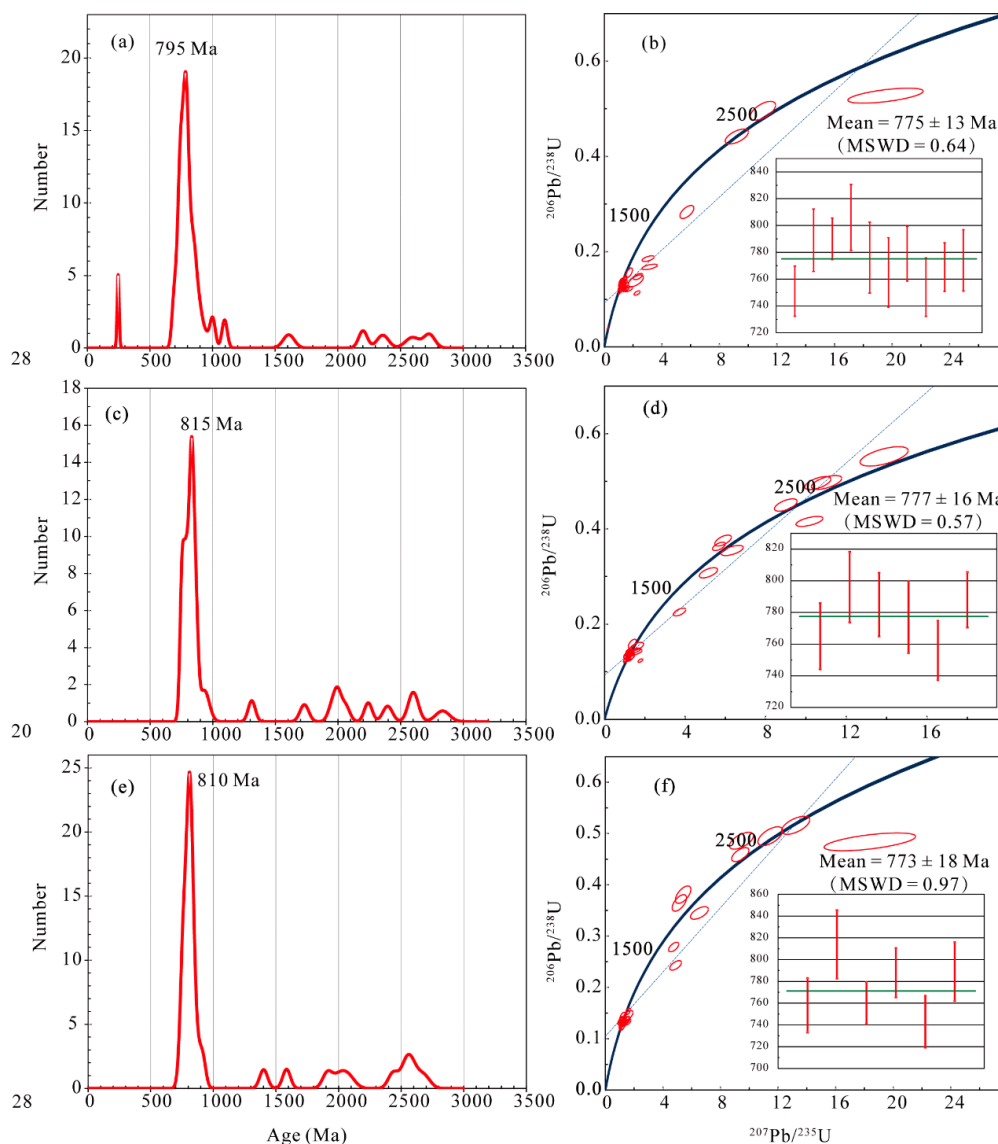
Figure 6. Historgams, Concordia and weighting mean ages of zircon grains from represented samples. (**a**) and (**b**) are of tuffaceous slate; (**c**) and (**d**) are of sandy slate; (**e**) and (**f**) are of gold-bearing quartz vein.

4.2. Major and Trace Element Compositions

The representative samples were analyzed for the major and trace element contents, and Tables S2 and S3 show the results. The sandy-slate samples have higher TiO_2, Al_2O_3, K_2O, and MgO contents, and lower SiO_2, and Na_2O than those of the tuffaceous slates, with mean SiO_2 contents of 65.5 wt. % and 72.4 wt. %, TiO_2 contents of 0.63 wt. % and 0.34 wt. %, Al_2O_3 contents of 17.4 wt. % and 14.4 wt. %, MgO contents of 0.82 wt. % and 0.61 wt. %, Na_2O contents of 2.65 wt. % and 3.0 wt. %, and K_2O contents of 4.53 wt. % and 3.72 wt. %, for the sandy-slate and tuffaceous slate, respectively. The quartz sample contains a high SiO_2 content of 91.0 wt. %, with a little Al_2O_3 and Fe_2O_3.

These samples have variable trace element compositions, although they have similar primitive mantle normalized patterns with the depletion of Cs, Nb, Hf, Sr, and Y, and enrichment of Ba, Th, U, Rb, La, and Ce (Figure 7a). In addition, most of the sandy slate samples have a high content of Au (mostly ranging from 0.019 to 0.252 ppm), which are higher than those of the tuffaceous samples (mostly lower than 0.005 ppm). In terms of the rare earth elements (REEs) compositions of these samples, the slate samples have higher REE contents, with ΣREEs of 194–366 ppm (mean = 266 ppm), than those of the tuffaceous slate and quartz samples with ΣREEs of 113–318 ppm (mean = 194 ppm) and 39.3

ppm, respectively. In addition, the enrichment of light rare earth elements (LREEs) and depletion of heavy rare earth elements (HREEs) characterize these samples, and these samples show similar chondrite-normalized patterns (Figure 7b). Furthermore, the sandy slate, tuffaceous slate, and quartz samples have negative Eu anomalies, with δEu of 0.49–0.73 (mean = 0.58), 0.43–0.73 (mean = 0.50), and 0.70, respectively.
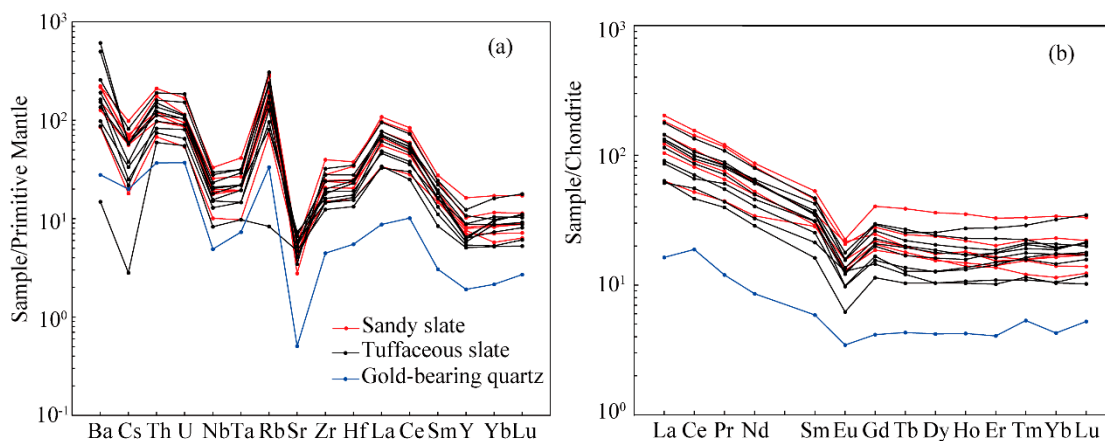
Figure 7. (**a**) Primitive mantle- and (**b**) chondrite-normalized patterns of samples from the Chaoyangzhai gold deposit. (a) and (b) are modified from [42,43], respectively.

Ten samples of gold-bearing quartz were assayed for the ore-forming metals analyses, and Table S3 displays the results. These gold-bearing quartz have variable Au (1.05–7.95 ppm), Cu (50–620 ppm), Pb (60–750 ppm), Zn (30–840 ppm), As (1500–7000 ppm), Sb (21.4–60.5 ppm), and Hg (0.02–0.07 ppm) contents (Figure 8).
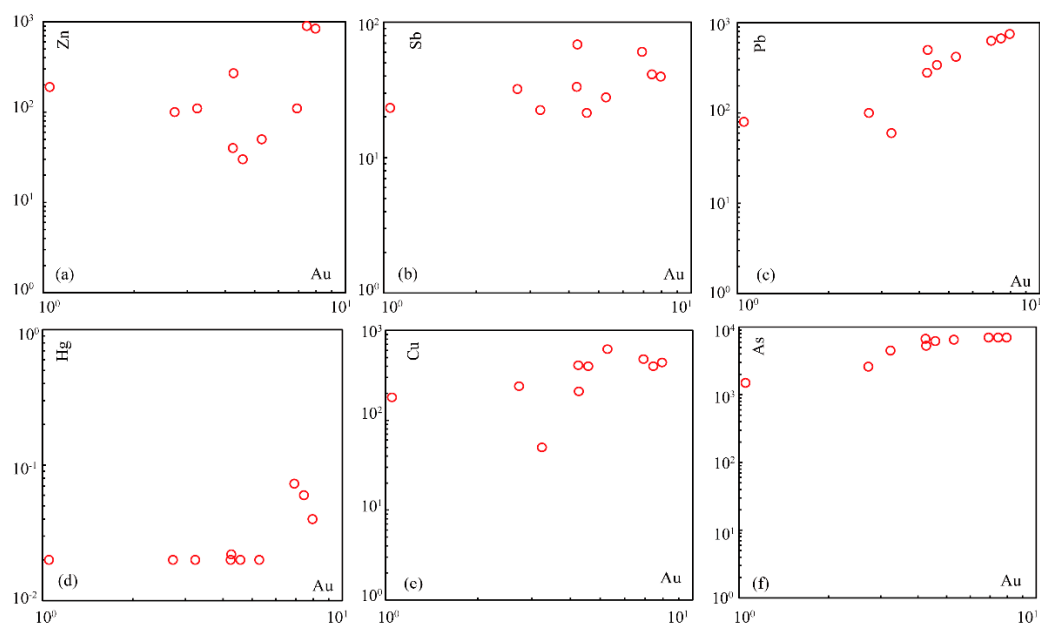
Figure 8. Geochemical plots of Au versus other ore-forming elements. All of the elements are given in ppm.

4.3. In Situ Sulfur Isotope Compositions

Table S4 presents the in situ LA-MC-ICP-MS analyses of sulfur isotopes. The measured $\delta^{34}S_{V\text{-}CDT}$ values of sulfides, which co-exit with the gold, range from +8.12‰ to +9.99‰, and from +9.78 to +10.78‰ for pyrite and arsenopyrite, respectively.

5. Discussion

5.1. Age and Source of Rocks from Qingshuijiang Formation

The Southeast Guizhou province is one of the significant gold producers in China, and numerous small- to large-sized gold deposits were explored in this region [7–10,17,31]. These deposits share the common feature that the quartz vein type ore bodies occur in Neoproterozoic epimetamorphic rocks [8–10,23]. In addition, these rocks mainly belong to the Neoproterozoic Xiajiang Group, which consists of the Longli, Pinglue, Qingshuijiang, and Fanzhao Formations. Gold-bearing ore bodies could occur in almost all of the epimetamorphic rocks of these Formations, with the Bake and the Chaoyangzhai gold deposits in rocks of the Qingshuijiang Formation, the Pingqiu gold deposit in rocks of the Fanzhao Formation, the Tonggu gold deposit in rocks of the Longli Formation, and the Jintou gold deposit in rocks of the Pinglue Formation (Figure 2). Previous studies have revealed that the deposited ages of Longli, Pinglue, Qingshuijiang, and Fanzhao Formations are 725 Ma, 733 Ma, 773.8 Ma, and 774 Ma, respectively [44,45]. In this study, the youngest detrital zircon ages of the tuffaceous- and sandy-slates of the Qingshuijiang Formation are 775 ± 13 Ma and 777 ± 16 Ma, respectively, which are consistent with the previous studies, constraining the deposited ages of the Qingshuijiang Formation [44,45]. In addition, the peak ages of the tuffaceous- and sandy-slates of the Qingshuijiang Formation are 799 Ma and 815 Ma, respectively, which is consistent with the intense Neoproterozoic magmatism of South China, triggered by the break-up of the Rodinia supercontinent [45–48]

Previous studies have indicated that the turbidite-hosted gold deposits in Southeast Guizhou might have a genetic relationship with the surrounding Neoproterozoic rocks [7–10]. In addition, these rocks are enriched in gold, which the high gold content of 0.019–0.252 ppm in the sandy slate of the Qingshuijiang formation confirmed. Therefore, the determination of the source for these rocks is one of the crucial issues in the genesis of these gold deposits. The geochemical compositions of the clastic sedimentary rocks have been widely used in determining the source and tectonic setting of such rocks [49–52]. Based on the discrimination diagram that was proposed by [49], most of the samples in this study plot were in the field of felsic igneous provenance (Figure 9a). In addition, the ΣREE vs. La/Yb diagram, also confirm the conclusion, since almost all of the samples were plotted in the field of granite (Figure 9b). The occurrence of abundant magmatic zircon grains in these rocks also supported this conclusion. Therefore, we proposed that these epimetamorphic rocks of Qingshuijiang Formation might originate from a magmatic source.
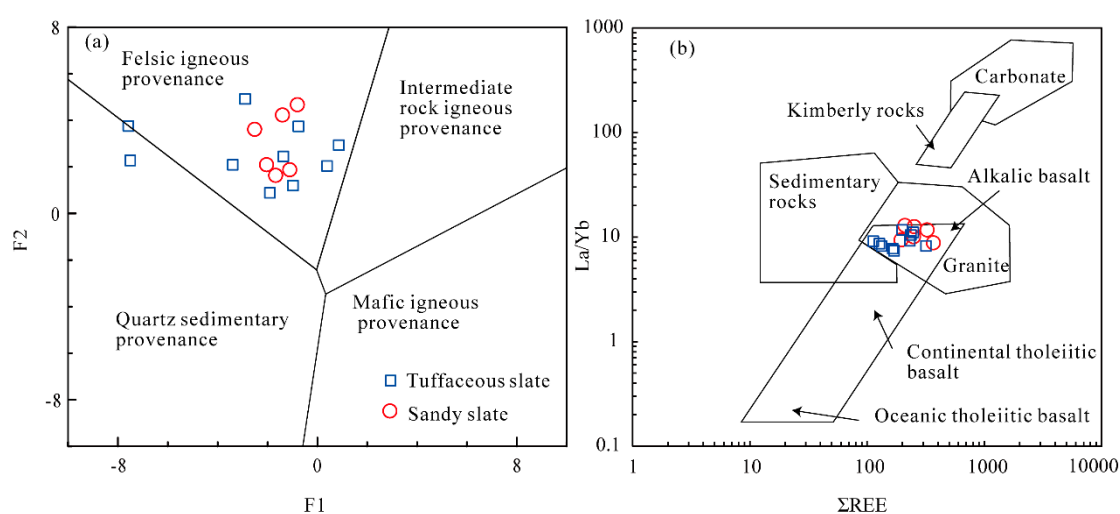

Figure 9. (**a**) F1 vs. F2 and (**b**) ΣREE vs. La/Yb plots for the rocks of Qingshuijiang Formation. Figure 9a,b are modified from [49] and [50], respectively. $F1 = -1.173TiO_2 + 0.607Al_2O_3 + 0.76TFe_2O_3 - 1.5MgO + 0.616CaO + 0.509Na_2O - 1.224K_2O - 9.09$; $F2 = 0.445TiO_2 + 0.07Al_2O_3 - 0.25TFe_2O_3 - 1.142MgO + 0.438CaO + 1.475Na_2O + 1.426K_2O - 6.861$.

5.2. Source of the Sulfur and Gold

Sulfides show distinct sulfur isotopic compositions in different geological systems; therefore, sulfur isotopes can be used as a key tracer in reflecting the ore-forming material sources of metallic mineral deposits [39,40,53–56]. *In situ* sulfur isotope analyses have been widely used in economic geology, because they can provide added evidence regarding the source of deposits [38,39,54,55]. Based on the occurrence of arsenopyrite and pyrite and the absence of magnetite and/or sulfates in the quartz vein type ore bodies, we proposed that the ore-forming fluid were reduced and the sulfur isotopic compositions of the sulfides reflects that of the ore-forming fluid system [57,58]. As shown in Table S4, the $\delta^{34}S_{V\text{-CDT}}$ values of pyrite and arsenopyrite range from +8.12‰ to +9.99‰ and from +9.78 to +10.78‰, respectively, which is consistent with the $\delta^{34}S_{V\text{-CDT}}$ values of the epimetamorphic rocks of the Neoproterozoic Qingshuijiang Formation (+9.27‰ to +12.44‰), as reported by [8]. Together with the sulfur isotopic compositions of the sulfides from the nearby gold deposits in this region, sulfur isotopes of the Chaoyangzhai gold deposit fall outside of the range of granitic and basaltic rocks, but within the interval of the metamorphic rocks of the Qingshuijiang (Figure 10). In addition, the quartz vein has similar primitive mantle normalized trace element patterns and chondrite normalized rare earth element patterns to the ore-hosting tuffaceous- and sandy-slate, which also indicates that the metal source of this deposit is likely of the tuffaceous- and sandy-slate. Therefore, we proposed that the sulfur source might be from the ore-hosting metamorphic rocks of the Qingshuijiang Formation. Furthermore, the detrital zircon ages of the tuffaceous- and sandy-slate have peaks of 775 ± 13 Ma and 777 ± 16 Ma, respectively, which are consistent with the U–Pb age of zircon grains (773 ± 18 Ma) from the gold-bearing quartz vein. It is indicated that the fluids might likely bring in these zircon grains of the gold-bearing quartz vein when they circulated in the gold-rich rocks.
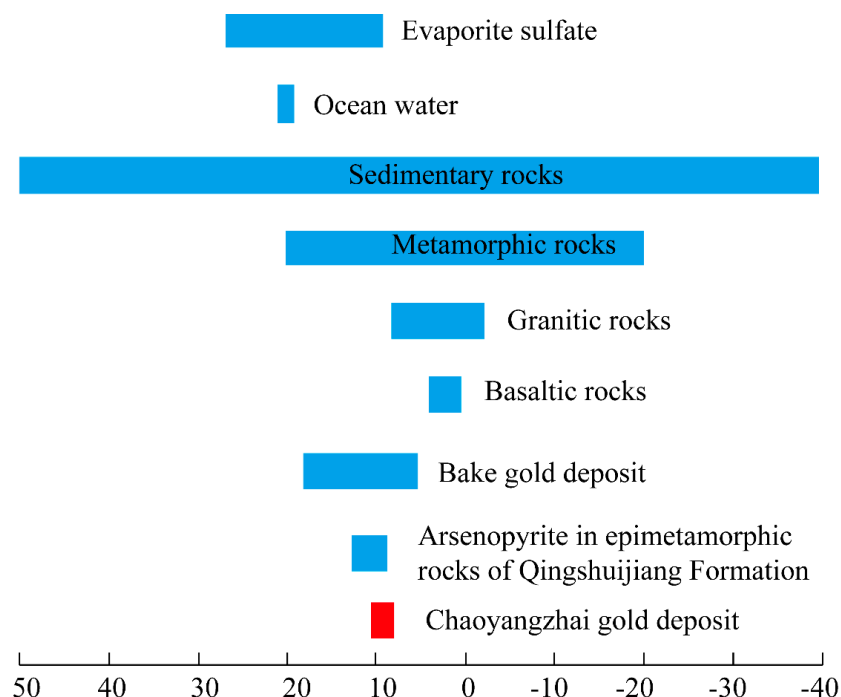

Figure 10. Sulfur isotopic compositions of the Chaoyangzhai gold deposit, showing some important sulfur reservoirs (modified from [59]). The sulfur isotopic data of arsenopyrite in epimetamorphic rocks of Qingshuijiang Formation and Bake deposit are from [8].

There are two types of metamorphic rocks of the Qingshuijiang Formation, the tuffaceous- and sandy-slate, however, which one is the source rocks of the Chaoyangzhai gold deposit? As shown in Table S2, the sandy-slate have a high content of Au (mostly ranging from 0.019 to 0.252 ppm), which is higher than those of the tuffaceous slate samples (mostly lower than 0.005 ppm). Thus, the most

probable source of the gold for the Chaoyangzhai gold deposit is the sandy slates of the Qingshuijiang Formation. The gold deposits confirmed this conclusion, which were also hosted in the Qingshuijiang Formation, for example, Bake, Jinning, and Kengtou gold deposits in this region [8–10]. Consequently, we proposed that the metal source of Chaoyangzhai gold deposit was mostly derived from the sandy slates of the Neoproterozoic Qingshuijiang Formation.

5.3. Genesis and Age of Turbidite-hosted Gold Deposits in Southeast Guizhou

A notable feature of these turbidite-hosted gold deposits, including the Chaoyangzhai gold deposit, is the major paragenetic association of native gold, arsenopyrite, and pyrite, which indicates that Au should be deposited in an Au-saturated fluid [60]. In addition, the arsenopyrite and pyrite could be the Au-carriers in the ore-forming fluid, and it was confirmed by numerous cases worldwide [61–66]. [61] reported that the Au content of arsenopyrite could be up to 65 ppm in the Moshan gold deposit, Southeast Guizhou. The same features were also observed in sulfides of other gold deposits in Southeast Guizhou [8,67]. The obvious positive correlation of the Au and As in this study confirmed this conclusion (Figure 8f). Previous studies furthermore proposed that gold was likely transported as the $Au(HS)_2{}^-$ in the fluid of low temperatures, low salinities, and low oxygen fugacities [60,68,69]. The homogenization temperatures of the Chaoyangzhai gold deposit range from 145 to 319 °C, with a cluster of ca. 200 °C, whereas the calculated salinities range from 0.18 to 17.9 wt. % NaCl equiv. (average = 7.5 wt. % NaCl equiv) (unpublished data). These temperatures and salinities of the fluids are similar to those of the Pingqiu gold deposit, Southeast Guizhou [9]. Together with the absence of the sulfate minerals and magnetite, it was proposed that these ore-forming fluids were of low temperature, low salinity, and low oxygen fugacity. As far as the source of these ore-forming fluids, numerous studies have been carried out on this issue; however, different viewpoints were proposed [4,9,61,70–73]. These viewpoints can be classified into three groups: metamorphic fluid [9], magmatic-hydrothermal fluid [4,70], and mixed fluid [61]. The viewpoint of magmatic-hydrothermal model might be unlikely as an explanation for the fluid source of these gold deposits since no coeval granitic intrusions were found in the Southeast Guizhou. In addition, the reported H–O isotopic data of these gold deposit are mainly in the range of the metamorphic fluids, although groundwater might be involved in the formation of these gold deposits [9,74]. Therefore, the metamorphic devolatilization model appears to be the best explanation of the origin of ore-forming fluids, and these metamorphic fluids could extract the gold and other metals from epimetamorphic rocks. Subsequently, accompanied by the change of physico-chemical conditions, gold was deposited in the suitable fractures, leading to the large-scale gold mineralization in Southeast Guizhou.

In terms of the ore-forming ages of these deposits, the reported metallogenic ages of these deposits could be summarized in two groups: Ordovician-Silurian (450–410 Ma) and Triassic-Jurassic (240–140 Ma), which is consistent with Caledonian and Indosinian-Yanshanian deformation, respectively [10]. The debate regarding the timing of the ore-forming events of these deposits might be caused by the lack of suitable minerals for dating, since pyrite and arsenopyrite are the associated minerals in these gold deposits. Recently, several ages of these gold deposits were reported, with ^{40}Ar-^{39}Ar age of 425.7 ± 1.7 Ma for the Pingqiu gold deposit [9], Re-Os age of 400 ± 11 Ma for the Jinjing gold deposit [7], and Re-Os age of 412 ± 21 Ma for the Bake gold deposit [23]. In addition, these ages are consistent with the ages of other gold deposits in the West Jiangnan Orogen Belt, for example, the Woxi Au deposit (423.2 ± 1.2 Ma, [23]), Banxi Sb-Au deposit (422.2 ± 0.2 Ma, [75]), and Jinshan Au deposit (406 ± 25 Ma, [76]). These reported high precision ages of these gold deposits indicate that the Caledonian is a significant gold mineralization epoch in South China, recording the Caledonian orogeny and the formation of these orogenic gold deposits in Southeast Guizhou.

6. Conclusions

Based on the geological, geochemical, geochronological studies on the Chaoyangzhai gold deposit, we draw the following conclusions:

(1) LA-ICP-MS zircon U–Pb dating of the gold-bearing quartz, tuffaceous- and sandy-slates display similar characteristics of age distribution, indicating that the zircons in the gold-bearing quartz could originate from the surrounding tuffaceous- and sandy-slates.

(2) Rocks of the Qingshuijiang Formation might be sourced from a felsic igneous provenance.

(3) Similar geochemical patterns between the surrounding tuffaceous- and sandy-slate and gold-bearing quartz illustrate that the Chaoyangzhai gold deposit might be sourced from the surrounding tuffaceous- and sandy-slate, supported by the sulfur isotopes of the arsenopyrite and pyrite.

(4) The sandy-slates have higher Au contents than the tuffaceous slate, indicating that the gold might be sourced from the sandy-slate rather than tuffaceous slate.

Supplementary Materials: The following are available online at http://www.mdpi.com/2075-163X/9/4/235/s1, Table S1. LA-ICP-MS zircon U–Pb dating of the host rocks and gold-bearing quartz veins from the Chaoyangzhai gold deposit. Table S2. Major and trace element compositions of the rocks from the Chaoyangzhai gold deposit. Table S3. Ore-forming element contents of the ore (ppm). Table S4. Sulfur isotopic compositions of the sulfides from the Chaoyangzhai gold deposit.

Author Contributions: H.T. and J.C. wrote the paper; J.C. and X.Y. designed the experiments; H.T. and X.Y. took part in the field investigation.

Conflicts of Interest: The authors declare no conflict of interest.

References

1. Horne, R.; Culshaw, N. Flexural-slip folding in the Meguma Group, Nova Scotia, Canada. *J. Struct. Geol.* **2001**, *23*, 1631–1652. [CrossRef]
2. Ramsay, W.; Bierlein, F.P.; Arne, D.C.; VandenBerg, A. Turbidite-hosted gold deposits of Central Victoria, Australia: their regional setting, mineralising styles, and some genetic constraints. *Ore Geol. Rev.* **1998**, *13*, 131–151. [CrossRef]
3. Windh, J. Saddle reef and related gold mineralization, Hill End gold field, Australia: Evolution of an auriferous vein system during progressive deformation. *Econ. Geol.* **1995**, *90*, 1764–1775. [CrossRef]
4. Lu, H.Z.; Wang, Z.G.; Chen, W.Y.; Wu, X.Y.; Zhu, X.Q.; Hu, R.Z. Turbidite hosted gold deposits in southeast Guizhou: Their structural control, mineralization characteristics, and some genetic constrains. *Miner. Depos.* **2006**, *4*, 369–387. (In Chinese)
5. Arne, D.C.; Bierlein, F.P.; Morgan, J.W.; Stein, H.J. Re–Os dating of sulfides associated with gold mineralization in Central Victoria, Australia. *Econ. Geol.* **2001**, *96*, 1455–1459. [CrossRef]
6. Molnar, F.; Middleton, A.; Stein, H.; O'Brien, H.; Lahaye, Y.; Huhma, H.; Pakkanen, L.; Johanson, B. Repeated syn- and post-orogenic gold mineralization events between 1.92 and 1.76 Ga along the Kiistala Shear Zone in the Central Lapland Greenstone Belt, northern Finland. *Ore Geol. Rev.* **2018**, *101*, 936–959. [CrossRef]
7. Wang, J.; Wen, H.; Li, C.; Zhang, J.; Ding, W. Age and metal source of orogenic gold deposits in Southeast Guizhou Province, China: Constraints from Re–Os and He–Ar isotopic evidence. *Geosci. Front.* **2019**, *10*, 581–593. [CrossRef]
8. Liu, A.; Jiang, M.; Ulrich, T.; Zhang, J.; Zhang, X. Ore genesis of the Bake gold deposit, southeastern Guizhou province, China: Constraints from mineralogy, in-situ trace element and sulfur isotope analysis of pyrite. *Ore Geol. Rev.* **2018**, *102*, 740–756. [CrossRef]
9. Liu, A.; Zhang, X.; Ulrich, T.; Zhang, J.; Jiang, M.; Liu, W. Geology, geochronology and fluid characteristics of the Pingqiu gold deposit, Southeastern Guizhou Province, China. *Ore Geol. Rev.* **2017**, *89*, 187–205. [CrossRef]
10. Xu, D.; Deng, T.; Chi, G.; Wang, Z.; Zou, F.; Zhang, J.; Zou, S. Gold mineralization in the Jiangnan Orogenic Belt of South China: Geological, geochemical and geochronological characteristics, ore deposit-type and geodynamic setting. *Ore Geol. Rev.* **2017**, *88*, 565–618. [CrossRef]
11. Goldfarb, R.J.; Groves, D.I. Orogenic gold: Common or evolving fluid and metal sources through time. *Lithos* **2015**, *233*, 2–26. [CrossRef]
12. Pitcairn, I.K.; Craw, D.; Teagle, D.A.H. Metabasalts as sources of metals in orogenic gold deposits. *Miner. Deposita* **2015**, *50*, 373–390. [CrossRef]

13. Phillips, G.N.; Powell, R. Origin of Witwatersrand gold: A metamorphic devolatilisation-hydrothermal replacement model. *Appl. Earth Sci.* **2011**, *120*, 112–129. [CrossRef]

14. Phillips, G.N.; Powell, R. Formation of gold deposits: a metamorphic devolatilization model. *J Metamorph. Geol.* **2010**, *28*, 689–718. [CrossRef]

15. Pang, J.T.; Dai, T.G. On the mineralization epoch of the Xuefeng gold metallogenic province. *Geol. Prospect.* **1998**, *34*, 37–41. (In Chinese)

16. Li, N.; Pirajno, F. Early Mesozoic Mo mineralization in the Qinling Orogen: An overview. *Ore Geol. Rev.* **2017**, *81*, 431–450. [CrossRef]

17. Tao, P.; Xiao, X.D.; Hu, C.L. The Au-bearing sedimentary sequences and theirimpact on the gold deposits in light metamorphic rock in the boundary of Hunan, Guizhou and Guangxi regions. *Geol. Sci. Technol. Inf.* **2009**, *28*, 100–104. (In Chinese)

18. Sun, J.; Shu, L.; Santosh, M.; Wang, L. Neoproterozoic tectonic evolution of the Jiuling terrane in the central Jiangnan orogenic belt (South China): Constraints from magmatic suites. *Precambrian Res.* **2017**, *302*, 279–297. [CrossRef]

19. Pan, X.; Hou, Z.; Zhao, M.; Chen, G.; Rao, J.; Li, Y.; Wei, J.; Ouyang, Y. Geochronology and geochemistry of the granites from the Zhuxi W–Cu ore deposit in South China: Implication for petrogenesis, geodynamical setting and mineralization. *Lithos* **2018**, *304*, 155–179. [CrossRef]

20. Wang, C.; Rao, J.; Chen, J.; Ouyang, Y.; Qi, S.; Li, Q. Prospectivity mapping for "Zhuxi-type" copper-tungsten polymetallic deposits in the Jingdezhen region of Jiangxi Province, South China. *Ore Geol. Rev.* **2017**, *89*, 1–14. [CrossRef]

21. Mao, J.; Xiong, B.; Liu, J.; Pirajno, F.; Cheng, Y.; Ye, H.; Song, S.; Dai, P. Molybdenite Re/Os dating, zircon U–Pb age and geochemistry of granitoids in the Yangchuling porphyry W–Mo deposit (Jiangnan tungsten ore belt), China: Implications for petrogenesis, mineralization and geodynamic setting. *Lithos* **2017**, *286*, 35–52. [CrossRef]

22. Huang, L.; Jiang, S. Highly fractionated S-type granites from the giant Dahutang tungsten deposit in Jiangnan Orogen, Southeast China: Geochronology, petrogenesis and their relationship with W-mineralization. *Lithos* **2014**, *202*, 207–226. [CrossRef]

23. Wang, J.; Wen, H.; Li, C.; Jiang, X.; Zhu, C.; Du, S.; Zhang, L. Determination of age and source constraints for the Bake quartz vein-type gold deposit in SE Guizhou using arsenopyrite Re–Os chronology and REE characteristics. *Geochem. J.* **2015**, *49*, 73–81. [CrossRef]

24. Deng, J.; Wang, Q. Gold mineralization in China: Metallogenic provinces, deposit types and tectonic framework. *Gondwana Res.* **2016**, *36*, 219–274. [CrossRef]

25. Lu, H.Z.; Wang, Z.G.; Wu, X.Y.; Chen, W.Y.; Zhu, X.Q.; Guo, D.J.; Hu, R.Z.; Keita, M. Turbidite-hosted gold Deposits in SE Guizhou Province, China: Their regional setting, structural control and gold mineralization. *Acta Geol. Sin.* **2005**, *79*, 98–105.

26. Tao, P.; Chen, Q.F.; Wang, L.; Hu, C.L. Location prediction of gold deposits for ore field grade in the Tianzhu-Jinping-Liping area, southeastern Guizhou, China: The method on potential assessment of mineral resources of low-exploration and study degree area. *J. Jilin Univ.* **2013**, *4*, 1235–1245. (In Chinese)

27. Goldfarb, R.J.; Taylor, R.D.; Collins, G.S.; Goryachev, N.A.; Orlandini, O.F. Phanerozoic continental growth and gold metallogeny of Asia. *Gondwana Res.* **2014**, *25*, 48–102. [CrossRef]

28. Zhou, T.H.; Goldfarb, R.J.; Phillips, G.N. Tectonics and distribution of gold deposits in China—an overview. *Miner. Deposita* **2002**, *37*, 249–282. [CrossRef]

29. Ren, J.S. The continental tectonics of China. *J. SE Asian Earth Sci.* **1996**, *13*, 197–204. [CrossRef]

30. Zeng, G.; Gong, Y.; Wang, Z.; Hu, X.; Xiong, S. Structures of the Zhazixi Sb–W deposit, South China: Implications for ore genesis and mineral exploration. *J. Geochem. Explor.* **2017**, *182*, 10–21. [CrossRef]

31. Liu, L.; Li, S.; Dai, L.; Suo, Y.; Liu, B.; Zhang, G.; Wang, Y.; Liu, E. Geometry and timing of Mesozoic deformation in the western part of the Xuefeng Tectonic Belt, South China: Implications for intra-continental deformation. *J. Asian Earth Sci.* **2012**, *49*, 330–338. [CrossRef]

32. Wiedenbeck, M.; Alle, P.; Corfu, F.; Griffin, W.L.; Meier, M.; Ober, F.; Von Quadt, A.; Roddick, J.C.; Speigel, W. Three natural zircon standards for U–Th–Pb, Lu–Hf, trace-element and REE analyses. *Geostand. Geoanal. Res.* **1995**, *19*, 1–23. [CrossRef]

33. Elhlou, S.; Belousova, E.; Griffin, W.L.; Pearson, N.J.; O Reilly, S.Y. Trace element and isotopic composition of GJ-red zircon standard by laser ablation. *Geochim. Cosmochim. Ac.* **2006**, *70*, A158. [CrossRef]

34. Liu, Y.; Gao, S.; Hu, Z.; Gao, C.; Zong, K.; Wang, D. Continental and Oceanic Crust Recycling-induced Melt-Peridotite Interactions in the Trans-North China Orogen: U–Pb Dating, Hf Isotopes and Trace Elements in Zircons from Mantle Xenoliths. *J. Petrol.* **2010**, *51*, 537–571. [CrossRef]

35. Liu, Y.; Hu, Z.; Gao, S.; Guenther, D.; Xu, J.; Gao, C.; Chen, H. In situ analysis of major and trace elements of anhydrous minerals by LA-ICP-MS without applying an internal standard. *Chem. Geol.* **2008**, *257*, 34–43. [CrossRef]

36. Andersen, T. Correction of common lead in U–Pb analyses that do not report ^{204}Pb. *Chem. Geol.* **2002**, *192*, 59–79. [CrossRef]

37. Sláma, J.; Košler, J.; Condon, D.J.; Crowley, J.L.; Gerdes, A.; Hanchar, J.M.; Horstwood, M.S.A.; Morris, G.A.; Nasdala, L.; Norberg, N.; et al. Plešovice zircon—A new natural reference material for U–Pb and Hf isotopic microanalysis. *Chem. Geol.* **2008**, *249*, 1–35. [CrossRef]

38. Bao, Z.; Chen, L.; Zong, C.; Yuan, H.; Chen, K.; Dai, M. Development of pressed sulfide powder tablets for in situ sulfur and lead isotope measurement using LA-MC-ICP-MS. *Int. J. MASS Spectrom.* **2017**, *421*, 255–262. [CrossRef]

39. Yuan, H.; Liu, X.; Chen, L.; Bao, Z.; Chen, K.; Zong, C.; Li, X.; Qiu, J.W. Simultaneous measurement of sulfur and lead isotopes in sulfides using nanosecond laser ablation coupled with two multi-collector inductively coupled plasma mass spectrometers. *J. Asian Earth Sci.* **2018**, *154*, 386–396. [CrossRef]

40. Chen, L.; Chen, K.; Bao, Z.; Liang, P.; Sun, T.; Yuan, H. Preparation of standards for in situ sulfur isotope measurement in sulfides using femtosecond laser ablation MC-ICP-MS. *J. Anal. Atom Spectrom.* **2017**, *32*, 107–116. [CrossRef]

41. Hoskin, P.W.O.; Schaltegger, U. The composition of zircon and igneous and metamorphic petrogenesis. *Rev. Mineral. Geochem.* **2003**, *53*, 27–62. [CrossRef]

42. Sun, S.S.; McDonough, W.F. Chemical and isotopic systematics of oceanic basalts: Implications for mantle compositions and processes. In *Magmatism in the Ocean Basins*; Saunders, A.D., Norry, M.J., Eds.; Geological Society of London Special Paper: London, UK, 1989; Volume 32, pp. 313–345.

43. Taylor, S.R.; McLennan, S.M. *Continental Crust: Its Composition and Evolution. An Examination of the Geochemical Record Preserved in Sedimentary Rocks*; Blackwell Science Inc.: Boston, MA, USA, 1985; p. 312.

44. Wei, Y.N.; Jiang, X.S.; Cui, X.Z.; Zhuo, J.W.; Jiang, Z.F.; Cai, J.J. Deteital zircon U–Pb ages of the Neoproterzoic Qingshuijiang Formation in Southeastern Guizhou and their geological significance. *J. Miner. Petrol.* **2015**, *35*, 61–71.

45. Wang, X.; Li, X.; Li, Z.; Li, Q.; Tang, G.; Gao, Y.; Zhang, Q.; Liu, Y. Episodic Precambrian crust growth: Evidence from U–Pb ages and Hf–O isotopes of zircon in the Nanhua Basin, central South China. *Precambrian Res.* **2012**, *222*, 386–403. [CrossRef]

46. Wang, L.; Griffin, W.L.; Yu, J.; O Reilly, S.Y. Precambrian crustal evolution of the Yangtze Block tracked by detrital zircons from Neoproterozoic sedimentary rocks. *Precambrian Res.* **2010**, *177*, 131–144. [CrossRef]

47. Wang, J.; Shu, L.; Santosh, M. U–Pb and Lu–Hf isotopes of detrital zircon grains from Neoproterozoic sedimentary rocks in the central Jiangnan Orogen, South China: Implications for Precambrian crustal evolution. *Precambrian Res.* **2017**, *294*, 175–188. [CrossRef]

48. Ma, X.; Yang, K.; Li, X.; Dai, C.; Zhang, H.; Zhou, Q. Neoproterozoic Jiangnan Orogeny in southeast Guizhou, South China: Evidence from U–Pb ages for detrital zircons from the Sibao Group and Xiajiang Group. *Can. J. Earth Sci.* **2016**, *53*, 219–230. [CrossRef]

49. Roser, B.P.; Korsch, R.J. Provenance signatures of sandstone mudstone suites determined using discriminant function-analysis of major-element data. *Chem. Geol.* **1988**, *67*, 119–139. [CrossRef]

50. Allegre, C.J.; Minster, J.F. Quantitative models of trace-element behavior in magmatic processes. *Earth Planet. Sc. Lett.* **1978**, *38*, 1–25. [CrossRef]

51. Anani, C.Y.; Bonsu, S.; Kwayisi, D.; Asiedu, D.K. Geochemistry and provenance of Neoproterozoic metasedimentary rocks from the Togo structural unit, Southeastern Ghana. *J. Afr. Earth Sci.* **2019**, *153*, 208–218. [CrossRef]

52. Lu, Y.; Zhu, W.; Ge, R.; Zheng, B.; He, J.; Diao, Z. Neoproterozoic active continental margin in the northwestern Tarim Craton: Clues from Neoproterozoic (meta) sedimentary rocks in the Wushi area, northwest China. *Precambrian Res.* **2017**, *298*, 88–106. [CrossRef]

53. Bauer, M.E.; Burisch, M.; Ostendorf, J.; Krause, J.; Frenzel, M.; Seifert, T.; Gutzmer, J. Trace element geochemistry of sphalerite in contrasting hydrothermal fluid systems of the Freiberg district, Germany: Insights from LA-ICP-MS analysis, near-infrared light microthermometry of sphalerite-hosted fluid inclusions, and sulfur isotope geochemistry. *Miner. Deposita* **2019**, *54*, 237–262.

54. Hu, X.; Tang, L.; Zhang, S.; Santosh, M.; Spencer, C.J.; Zhao, Y.; Cao, H.; Pei, Q. In situ trace element and sulfur isotope of pyrite constrain ore genesis in the Shapoling molybdenum deposit, East Qinling Orogen, China. *Ore Geol. Rev.* **2019**, *105*, 123–136. [CrossRef]

55. Li, X.; Zhao, K.; Jiang, S.; Palmer, M.R. In-situ U–Pb geochronology and sulfur isotopes constrain the metallogenesis of the giant Neves Corvo deposit, Iberian Pyrite Belt. *Ore Geol. Rev.* **2019**, *105*, 223–235. [CrossRef]

56. Liang, J.; Li, J.; Sun, W.; Zhao, J.; Zhai, W.; Huang, Y.; Song, M.; Ni, S.; Xiang, Q.; Zhang, J.; et al. Source of ore-forming fluids of the Yangshan gold field, western Qinling orogen, China: Evidence from microthermometry, noble gas isotopes and in situ sulfur isotopes of Au-carrying pyrite. *Ore Geol. Rev.* **2019**, *105*, 404–422. [CrossRef]

57. Downes, P.M.; Seccombe, P.K.; Carr, G.R. Sulfur- and lead-isotope signatures of orogenic gold mineralisation associated with the Hill End Trough, Lachlan Orogen, New South Wales, Australia. *Miner. Petrol.* **2008**, *94*, 151–173. [CrossRef]

58. Jia, Y.F.; Li, X.; Kerrich, R. Stable isotope (O, H, S, C, and N) systematics of quartz vein systems in the turbidite-hosted Central and North Deborah gold deposits of the Bendigo cold field, Central Victoria, Australia: Constraints on the origin of ore-forming fluids. *Econ. Geol.* **2001**, *96*, 705–721. [CrossRef]

59. Hoefs, J. *Stable Isotope Geochemistry*; Spring: Berlin/Heidelberg, Germany, 2009; pp. 71–73.

60. Zhu, Y.; An, F.; Tan, J. Geochemistry of hydrothermal gold deposits: A review. *Geosci. Front.* **2011**, *2*, 367–374. [CrossRef]

61. Zhang, J.; Yu, D.L.; Zhang, X.Y.; Yang, Y.J. Geochemical characteristice and modes of occurrence of gold in the Moshan-Youmaao gold deposit of Tianzhu, Guizhou. *J. Guizhou Univ. Technol.* **1997**, *26*, 43–49. (in Chinese).

62. Zhang, H.; Zhu, Y. Mechanism of gold precipitation in the Gezigou gold deposit, Xinjiang, NW China: Evidence from fluid inclusions and thermodynamic modeling. *J. Geochem. Explor.* **2019**, *199*, 60–74. [CrossRef]

63. Song, G.X.; Cook, N.J.; Wang, L.; Qin, K.Z.; Ciobany, C.; Li, G.M. Gold behavior in intermediate sulfidation epithermal systems: A case study from the Zhengguang gold deposit, Heilongjiang Province, NE-China. *Ore Geol. Rev.* **2019**, *106*, 446–462. [CrossRef]

64. Kovalev, K.R.; Kalinin, Y.A.; Naumov, E.A.; Kolesnikova, M.K.; Korolyuk, V.N. Gold-bearing arsenopyrite in eastern Kazakhstan gold-sulfide deposits. *Russ. Geol. Geophys.* **2011**, *52*, 178–192. [CrossRef]

65. Cook, N.J.; Ciobanu, C.L.; Meria, D.; Silcock, D.; Wade, B. Arsenopyrite-Pyrite Association in an Orogenic Gold Ore: Tracing Mineralization History from Textures and Trace Elements. *Econ. Geol.* **2013**, *108*, 1273–1283. [CrossRef]

66. Salvi, S.; Velasquez, G.; Miller, J.M.; Beziat, D.; Siebenaller, L.; Bourassa, Y. The Pampe gold deposit (Ghana): Constraints on sulfide evolution during gold mineralization. *Ore Geol. Rev.* **2016**, *78*, 673–686. [CrossRef]

67. Zhao, J.; Liang, J.L.; Li, J.; Ni, X.S.; Xiang, Q.R. Genesis and metallogenic model of the Shuiyindong gold deposit, Guizhou Province: Evidences from high-resolution multi-element mapping and in situ sulfur isotopes of Au-carrying pyrites by NanoSIMS. *Earth Sci. Fron.* **2018**, *25*, 157–167. (in Chinese).

68. Fan, H.R.; Zhai, M.G.; Xie, Y.H.; Yang, J.H. Ore-forming fluids associated with granite-hosted gold mineralization at the Sanshandao deposit, Jiaodong gold province, China. *Miner. Deposita* **2003**, *38*, 739–750. [CrossRef]

69. Yoo, B.C.; Lee, H.K.; White, N.C. Mineralogical, fluid inclusion, and stable isotope constraints on mechanisms of ore deposition at the Samgwang mine (Republic of Korea)—A mesothermal, vein-hosted gold-silver deposit. *Miner. Deposita* **2010**, *45*, 161–187. [CrossRef]

70. Wu, W.M.; Liu, J.Z.; Wang, Z.P.; Yu, D.L. Indicative significance of H–O isotope and fluid inclusion in ore-forming fluid of Pingqiu gold mine, Guizhou province. *Gold Sci. Technol.* **2015**, *23*, 30–36.

71. Seward, T.M.; Williams-Jones, A.E.; Migdisov, A.A. The chemistry of metal transport and deposition by ore-forming hydrothermal fluids. In *Treatise on Geochemistry*, 2nd ed.; Turekian, K., Holland, H., Eds.; Elsevier: New York, NY, USA, 2014; Volume 13, pp. 29–57.

72. Williams-Jones, A.E.; Bowell, R.J.; Migdisov, A.A. Gold in solution. *Elements* **2009**, *5*, 281–287. [CrossRef]

73. Pal'yanova, G. Physicochemical modeling of the coupled behavior of gold and silver in hydrothermal processes: Gold fineness, Au/Ag ratios and their possible implications. *Chem. Geol.* **2008**, *255*, 399–413. [CrossRef]

74. Tian, H.D.; Huang, D.G.; Yu, Q.P. Analyses on gelogic characters and genesis of Kengtou gold deposit in Tianzhu, Southeast Guizhou. *Guizhou Geol.* **2011**, *28*, 265–271. (in Chinese).

75. Peng, J.T.; Hu, R.Z.; Zhao, J.H.; Fu, Y.Z.; Lin, Y.X. Scheelite Sm–Nd dating and quartz Ar–Ar daing of Au–Sb–W depos it in Woxi, west Hunan. *Chin. Sci. Bull.* **2003**, *48*, 1976–1981. (in Chinese). [CrossRef]

76. Wang, X.Z.; Liang, H.Y.; Shan, Q.; Cheng, J.P.; Xia, P. Metallogenic age of the Jinshan gold deposit and Caledonian gold mineralization in South China. *Geo. Rev.* **1999**, *45*, 19–25. (in Chinese).